

Polymerizable channel-like stacks derived from cyclic tetrameric diacetylenes

Oleg V. Kulikov ^{a,b,*}, Arshad Mehmood ^c, Yulia V. Sevryugina ^c

^a Huntsman Advanced Materials, The Woodlands, TX, 77381, USA

^b Department of Chemistry, Massachusetts Institute of Technology, Cambridge, MA, 02139, USA

^c Department of Chemistry, Texas Christian University, Fort Worth, TX, 76129, USA



ABSTRACT

A small series of cyclic diacetylenes has been synthesized and tested by scanning electron microscopy (SEM), single crystal X-ray diffraction, and atomic force microscopy (AFM) to examine their ability to form arrangements of discrete molecules in the solid state. Examining solid state structures clearly demonstrated propensity of diacetylene tetramers to form channel-like stacks. Remarkably, cyclotetradiyne DA-4 monomer tends to produce two types of nano-tubular motifs (*i.e.*, the channel-like arrangement with solvent matrix inside and unprecedented flattened nano-tube incorporated no solvent guest molecules) which is indicative of the weak C–H/π interactions dominating and directing the stacking in such simplistic diacetylene cyclic systems. Noteworthy, DA-4 molecules may be crystallized from organic solvents into birefringent branched patterns revealed by Polarized Optical Microscopy (POM) and twisted ribbons of both handedness as evidenced by SEM data. We hypothesize that all these secondary structures may arise from the bundling the individual stacks discovered by single crystal X-ray analysis. Overall, engineering the elongated motifs may open up new opportunities for the future applications such as a rational design of synthetic ion channels and carriers, synthesis of the covalent polymeric nanotubes, *etc.*

1. Introduction

Ability of the various macrocycles and macroheterocycles to form channel-like motifs is well-established [1–12] which also includes stabilization of assemblies with functional polydiacetylenes. [13] Among those, an interesting and promising class of macrocycles prone to solid state stacking and topochemical polymerization is represented by dehydro [24]annulenes [11] and cyclic phenylacetylenes polymerizable under pressure [14]. Over the years, there has been an overwhelming interest in developing various polydiacetylenes (PDAs) based platforms [15], *i.e.*, gels, films, vesicles, mostly due to their unique optical properties [16] which allowed to use them in a large variety of applications, such as colorimetric sensors (blue/red phase switching) [17], colorimetric supramolecular gels [18a], diacetylene based multivalent glycol-polymers for high affinity lectin binding [18b], sensors as quality indicators in food packaging [19], chemosensors for colorimetric detection of cadmium ions [20], electromechanical actuators [21a], ultrastrong bioorthogonal Raman probes for targeted live-cell Raman imaging [21b], highly sensitive PDA ensembles for biosensing and bio-imaging [21c]. In addition to that, this widely investigated family of conjugated polymers attracted much attention due to their remarkable semiconducting and optoelectronic properties [22]. Interestingly,

topochemical polymerization of diacetylenes can be tuned and is closely related to the length of peripheral alkyl side groups exhibiting odd/even effect on polymerization [23]. In contrast to numerous examples of the linear PDA backbones described above, slightly less ubiquitous cyclic oligodiyne monomers may provide an access to polydiacetylene scaffolds bearing no peripheral side chains. Thus, understanding the underlying factors which impact cyclic diacetylenes' assembly in solid state, such as effect of inner and outer alkyl chains, crystallization solvent, appeared to be critical for successful topochemical polymerization. For instance, authors demonstrated the viability of synthetic approach towards graphene nanoribbons by using 1,4-diarylbutadiyne monomers that are initially converted to polydiacetylenes via topochemical polymerization in the crystal with subsequent cyclization and aromatization steps finally leading to graphene nanoribbons [24a]. Also, researchers [24b] described the solid cyclically-bound ladder polymers obtained from cyclic tetramers with no peripheral alkyl side chains. Thus, crystal-controlled 1,4-addition polymerization of cyclic tetramer afforded hydrocarbon organic nanotubes with carbon atoms connectivity favorable for the next extrusion step leading to carbon nanotube [24c].

In the present work, a series of cyclic diacetylenes (DA-3–DA-6) has been prepared and characterized by means of scanning electron microscopy (SEM) and single crystal X-ray analysis (X-ray) in a context of both

* Corresponding author. Huntsman Advanced Materials, The Woodlands, TX, 77381, USA.

E-mail addresses: Oleg.Kulikov@huntsman.com, okulikov@mit.edu (O.V. Kulikov).

UV- and thermally induced topochemical polymerization. Herein, we report synthesis and solid state polymerization of some cyclic oligodiynes, namely, cyclotetracosa-1,3,9,11,17,19-hexayne (**DA-3**), cyclodo triaconta-1,3,9,11,17,19,25,27-octayne (**DA-4**), cyclotetraconta-1,3,9, 11,17,19,25,27,33,35-decayne (**DA-5**) which hold a great potential for constructing tunnel-like arrangements as a result of non-covalent CH $\cdots \pi$ interactions. Structurally similar diacetylene scaffolds were shown to be specifically aligned with respect to each other which is an important prerequisite for topochemical polymerization [25]. We reasoned that using aforementioned cyclic diacetylenes to construct polymerizable channel-like frameworks is advantageous as their molecules have no bulky substituents preventing tight packing of individual channels in a bundle, thus, giving a rise to highly ordered arrangements which is beneficial for high density PDA materials. In particular, **DA-4** cyclotetraadiyne monomer [26a] represents considerable interest as its molecules are prone to self-organize into stackable motif in the solid state (e.g., needlelike crystals obtained from 25% (v/v) CHCl₃-petroleum ether by room temperature evaporation) which was further polymerized^{26b,c} using 50 Mrad of ⁶⁰Co γ -radiation. Likewise, abovementioned diacetylene tetramer, some alternative synthetically made backbones have shown to afford columnar polydiacetylenes having two parallel PDA chains that run parallel down opposite sides of a channel [27a] which may be of interest for the formation of highly conductive organic materials. This manuscript details morphological characterization of uncommon class of cyclic diacetylenes bearing no peripheral substituents (Scheme 1, Figure S1), thus, representing significant interest due to their ability to self-organize in a crystal lattice into tightly packed bundled channel-like arrangements, which consequently influences higher order organization, such as right and left-handed ribbons and fiber-like secondary PDA structures.

2. Results and discussion

2.1. Single crystal X-ray studies of channel-forming **DA-4** macrocycle

To understand assembly factors leading to columnar arrangements, we investigated solid state structures of **DA-3**–**DA-5** cyclic diacetylenes. We presume that cyclic tetramer diacetylenes with C≡C–C≡C bond segments may be stacked as was shown for cyclic tetraadiyne by growing crystals from specific solvent mixture [26b]. Having interstitial solvent molecules inside the stack of **DA-4** diacetylenes seemed to be important. We discovered in this study that solid state packing of **DA-4** macrocycles can be tuned by using different solvents. Thus, macrocyclic building blocks were shown to form extended, stackable arrays when crystallized from toluene, mesitylene, 1,4-dioxane, and CHCl₃/EtOH solvent mixture (Fig. 1, S2–S22). For all structures inspected by X-ray, measured packing parameters are somewhat close to repeat distance $d_1 = 4.9 \text{ \AA}$, the contact distance $d_2 = 3.5 \text{ \AA}$, and tilt angle $\theta = 45^\circ$ reported for butadiyne topochemical polymerization [11] as well as for single-crystal-to-single-crystal transformation of diacetylenes to PDA [27a], $d_1 = 4.99 \text{ \AA}$, $d_2 = 3.58 \text{ \AA}$, and tilt angle $\theta = 41.6^\circ$, correspondingly. Those parameters are also reminiscent of distances found in crystal structure of macrocyclic naphthalene diacetylene nanotubes [27b] ($d_1 = 5.29 \text{ \AA}$, $d_2 = 3.79 \text{ \AA}$, and tilt angle $\theta = 45.65^\circ$). Remarkably, macrocyclic diacetylene-terthiophene plate-like polymerizable co-crystal [27c]

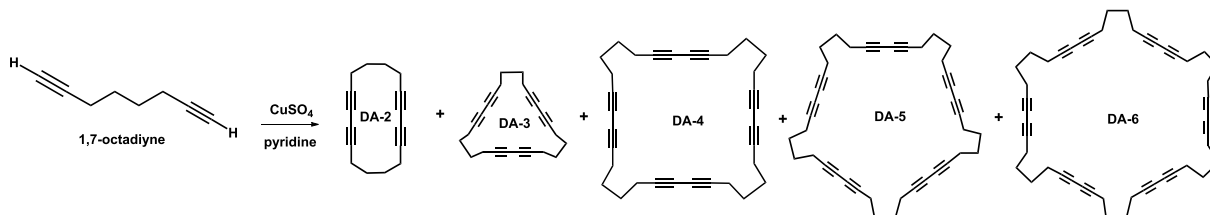
showed appreciably greater distance values, i.e., $d_1 = 10.31 \text{ \AA}$, $d_2 = 8.12 \text{ \AA}$, and tilt angle $\theta = 45.4^\circ$, which are still considered to be close-to-ideal packing parameters [27b] preferred for topochemical polymerization. Adjusting the size of macrocyclic diacetylenes to ensure perfect columnar stacking is certainly a challenge in the crystal engineering. Thus, authors [27d] successfully constructed photo-irradiation polymerizable tubular assembly from L-glutamic acid and *trans*-1,4-cyclohexanediol macrocyclic diacetylene compound with no peripheral aromatic segments as the result of intermolecular hydrogen bonding.

Single crystal X-ray studies revealed that individual **DA-4** diacetylenes in the crystal lattice are pre-organized in a way favorable for topochemical polymerization with d_1 ranging from 4.94 to 5.03 \AA , d_2 ranging from 3.42 to 3.69 \AA and tilt angle $\theta = 43.3\text{--}47.8^\circ$. We attribute unremarkable differences in diacetylene geometries to the crystal packing forces due to the solvent effect. All the **DA-4** structures demonstrated non-planar conformation (Figures S2, S5, S9, and S13). Stacking the discrete cyclic diacetylenes afforded channel-like structures with interstitial solvent molecules occupying the free volume inside those arrangements (Fig. 1, S3, S4, S6–S8, S10–S12).

We attribute this to weak C–H/ π as well as van der Waals interactions which may be stabilizing channel-like arrangement. The latter may optionally incorporate template solvent molecules.

Apparently, **DA-4** channel-like motif obtained from CHCl₃/EtOH solvent mixture is vastly different from those outlined in Fig. 1 as no template solvent molecules were detected inside the assembly (Fig. 2, panels a and b). Therefore, CHCl₃/EtOH derived nanotube is somewhat flattened compared to the rest of **DA-4** assemblies obtained from other solvents. Since AFM specimen was prepared using the same EtOH/CHCl₃ stock solution from which crystals for single crystal X-ray analysis were grown, we infer that organization of **DA-4** molecules in the tubular morphologies at nano-scale level may mimic their assembly in crystal lattice. Furthermore, partial crystal packing diagram suggested that dozens of individual nanotubes can be bundled into fiber-like aggregates with diameter less than 25 nm easily identifiable on AFM phase diagram (Fig. 2, panels c, d; S23). More nano-tubular stacking diagrams can be found in ESI (Figures S4, S7, S8, S11, S12, S15), thus, providing clear evidence that such bundles is a common motif for **DA-4** type diacetylenes, at least, in the crystal lattice. Given the proximity of adjacent C_{1'} and C₄ carbon atoms as well as geometrical orientation of the individual macrocycles favorable for formation of the new double bond (Figs. 1 and 2), polymerization seemed likely to occur under irradiation or at high temperatures.

Thus, the choice of crystallization solvent plays a significant role in constructing and stabilizing the **DA-4** monomer reactive phase. Analysis of a variety of self-assembled structures examined by single crystal X-ray analysis is suggestive that **DA-4** diacetylenes are prone to topochemical polymerization. Unlike aforementioned structures, packing diagrams of **DA-3** and **DA-5** diacetylenes did not reveal apparent channel-like constructs (Figures S17–S19, S21–S22) which proved that **DA-4** diacetylenes have optimal geometry and cycle dimensions that enable stacking of individual rings into the nano-tubes. We speculate that **DA-3** molecule represents constrained geometries whereas both **DA-5** and **DA-6** diacetylenes with much larger cavity have many more degrees of conformational freedom which complicates pre-alignment of the neighboring diacetylene units needed for columnar organization. For



Scheme 1. Synthesis of cyclic diacetylenes from 1,7-octadiyne using oxidative coupling reaction.

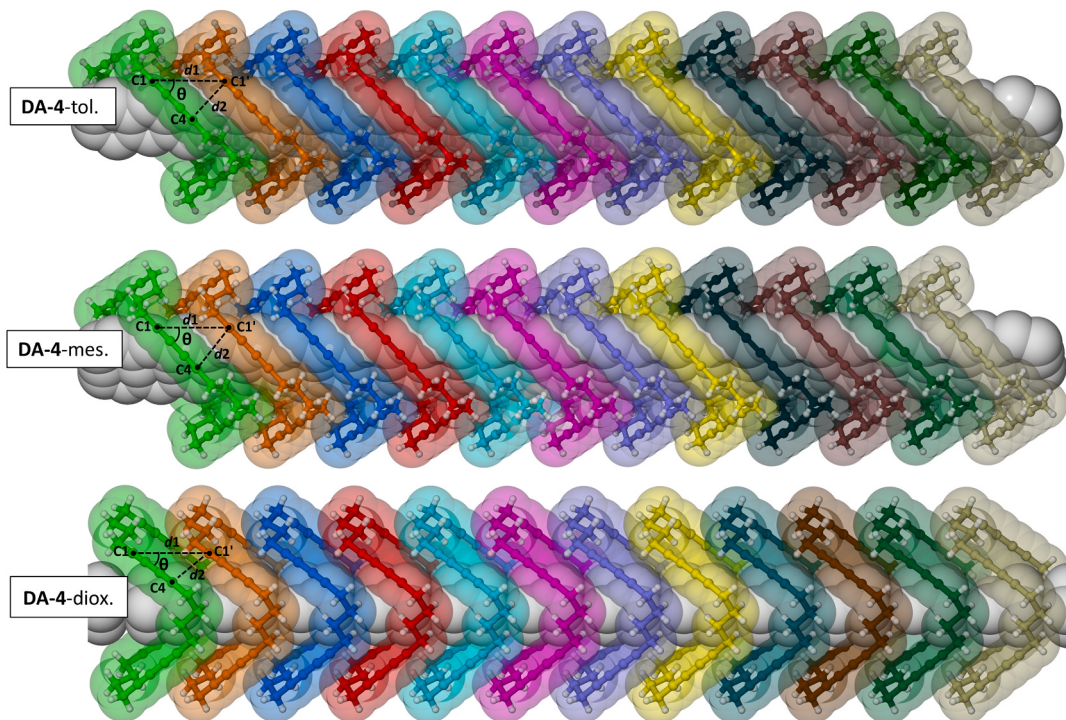


Fig. 1. Shown here are channel-like motifs assembled from twelve individual segments (cycles) as potentially polymerizable structures (disordered solvent molecules inside the assemblies shown as white overlapping spheres). Arrangement parameters, DA-4 from toluene, CCDC 1852360: $\theta = 44.6^\circ$, $d_1 = 5.03 \text{ \AA}$, $d_2 = 3.54 \text{ \AA}$; DA-4 from mesitylene, CCDC 1852358: $\theta = 47.8^\circ$, $d_1 = 4.94 \text{ \AA}$, $d_2 = 3.69 \text{ \AA}$; DA-4 from 1,4-dioxane, CCDC 1852361: $\theta = 43.3^\circ$, $d_1 = 4.99 \text{ \AA}$, $d_2 = 3.42 \text{ \AA}$

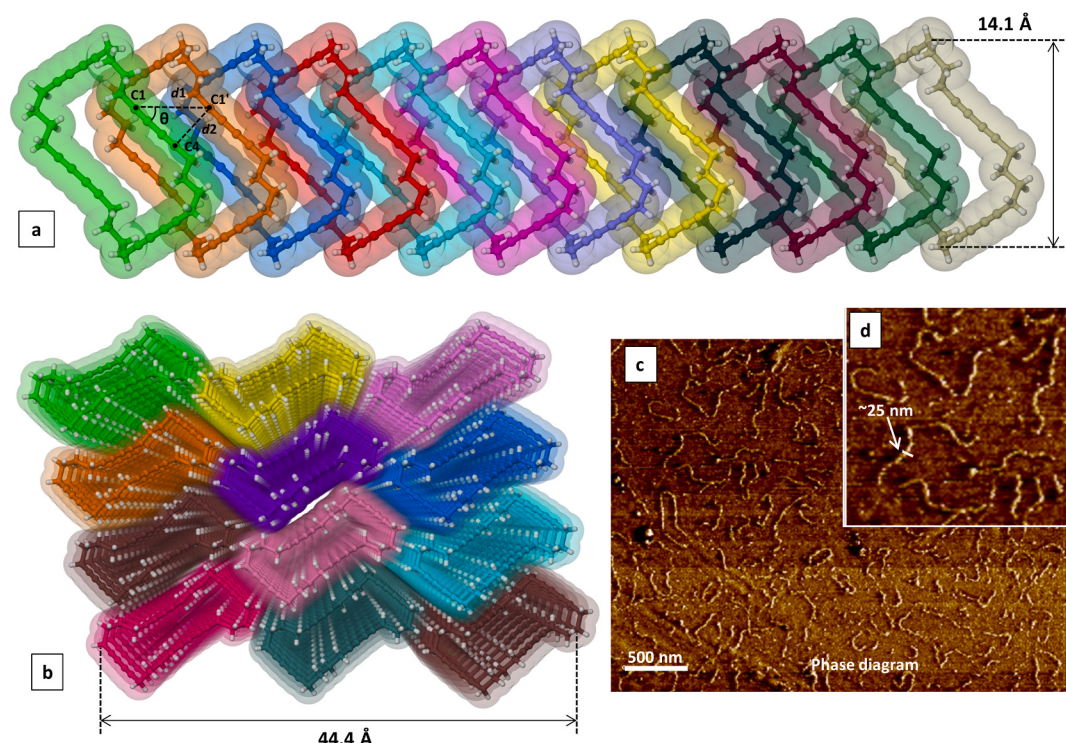


Fig. 2. Shown here is DA-4 cyclic monomer from $\text{CHCl}_3/\text{EtOH}$, CCDC 1852357: $\theta = 44.4^\circ$, $d_1 = 5.11 \text{ \AA}$, $d_2 = 3.58 \text{ \AA}$. The tubular “solvent-free” motif is formed from twelve individual diacetylene tetramers (panel a) which are packed in a channel-like fashion (panel b). Panel c represents AFM phase diagram of fibrous network obtained by depositing DA-4 stock in $\text{CHCl}_3/\text{EtOH}$ on Si-wafer and annealed at 100°C .

instance, adjacent **DA-3** molecules laying on the same axis demonstrated repeat distance (d_1) of 8.45 Å (Figure S17) likewise **DA-5** exhibited $d_1 = 10.00$ Å (Figure S21) which exceeded the typical separation distance observed in **DA-4** diacetylenes (~5 Å).

2.2. The 1,4-addition polymerization of the cyclic diacetylenes

Importantly, all investigated diacetylenes demonstrated some propensity to develop an intense colour over extended period of time even without being exposed to UV-light or annealed at elevated temperatures which can be best explained by the formation of a system of conjugated C=C-C≡C bonds. However, this is more pronounced in case of **DA-4** molecules due to their unique geometry and inter-cycle separation of ~5 Å, which is optimal for polymerization. Noticeably, pXRD plot of starting **DA-4** material featured numerous 2θ maxima (Figure S24) implying high crystallinity of **DA-4** monomer. In fact, all the cyclic diacetylenes after isolation in a pure form shall be stored at low temperatures to prevent them from self-polymerizing which is evident by the presence of characteristic C=C band at ~1700 cm⁻¹ in their respective FT-IR spectra, Figures S25–S30. Analysis of Raman spectra recorded at 533 nm led us to a conclusion about partial polymerization of **DA-4** monomer in the bulk (Fig. 3, panel a) featuring an intense line at 1493 nm associated with a double bond in the polymer backbone which is practically absent in the **DA-4** monomer [26c].

Another characteristic band at 2102 cm⁻¹ may be attributed to an

alternating triple bond in PDA structure. Those values match up closely reported Raman intense vibration at 2105 cm⁻¹ ($\nu_{C\equiv C}$) and 1490 cm⁻¹ ($\nu_{C=C}$) in the polymer derived from cyclotetradiyne **DA-4** monomer, which corresponds to the multiple-bond vibrations in the backbone [26c]. These observations are in accordance with FT-IR data for polymerized **DA-4** specimens (Fig. 3b) displaying the massive peak at ~1700 cm⁻¹ which belongs to C=C stretch not seen in starting **DA-4** monomer, blue line. In fact, polymerization can be achieved by using UV-light, thermal annealing, or even by leaving **DA-4** monomer in a solvent such as chloroform for extended periods of time, which led to the formation of insoluble polymer (Figure S28). Apparently, LED-UV source appeared to be a convenient and efficient way to induce topochemical polymerization (Fig. 3b and S31) as the most of **DA-4** monomer was transformed into the respective PDA species. However, our primary focus here is on transformation of channel-like arrangement of **DA-4** cyclic tetradiyne into covalently linked nano-tubular structure in the solid state, therefore, other potentially polymerizable diacetylene phases derived from **DA-3**, **DA-5**, and **DA-6** diacetylenes are not discussed in this paper. Thus, synthesis of PDAs was successfully accomplished using crystal-controlled 1,4-addition polymerization of diacetylene groups of **DA-4** monomer to give a rise to organic nanotube with covalent linkages between discrete cycles. The structure of PDA backbone can be perceived as individual hydrocarbon cycles stitched up by alternating double and triple bonds to form infinite covalent network shown in Fig. 4a panel. We surmise that our choice of analytical

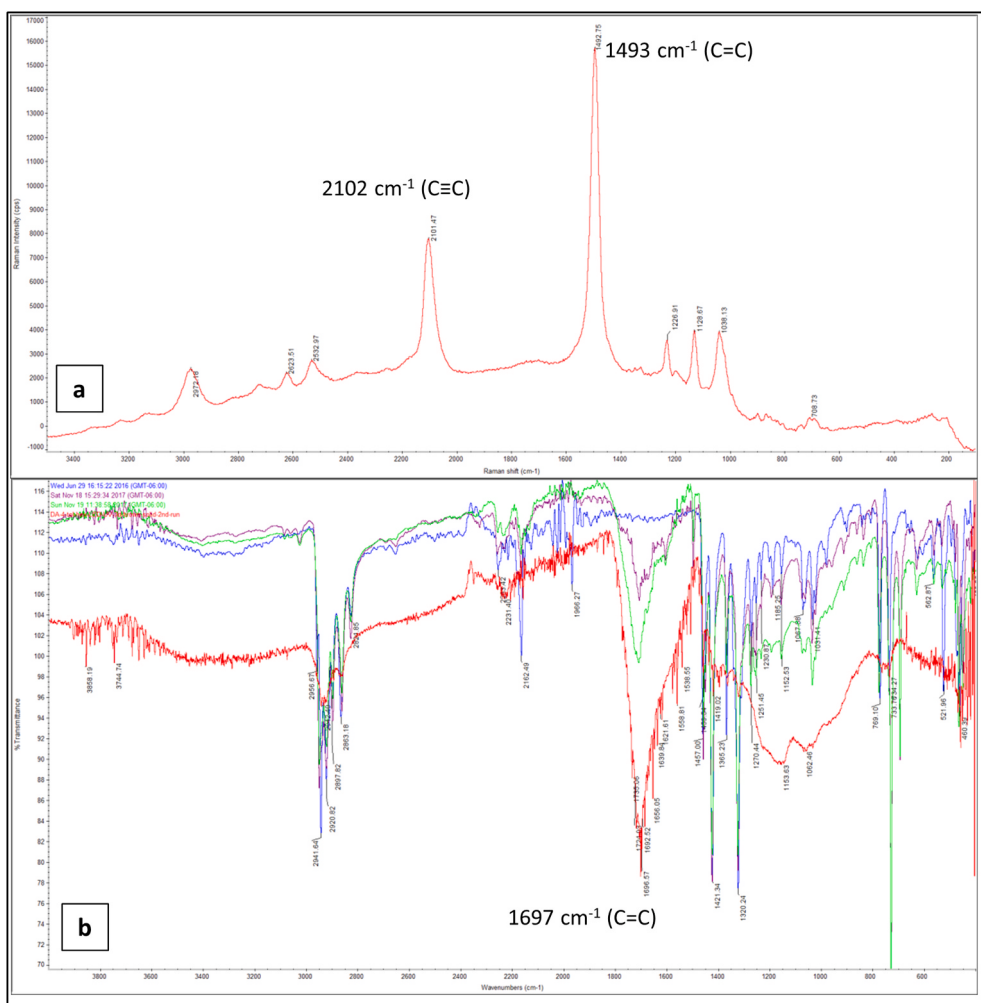


Fig. 3. Raman spectrum of **DA-4** cyclic diacetylene irradiated with UV-254 nm light (panel a) and FT-IR spectra of **DA-4** (panel b) crystallized from toluene and exposed to UV-light (legend: starting **DA-4** material — blue plot, irradiated by UV-254 nm overnight — magenta plot, irradiated by both UV 254 nm and 365 nm — green plot, irradiated with LED UV-source — red plot).

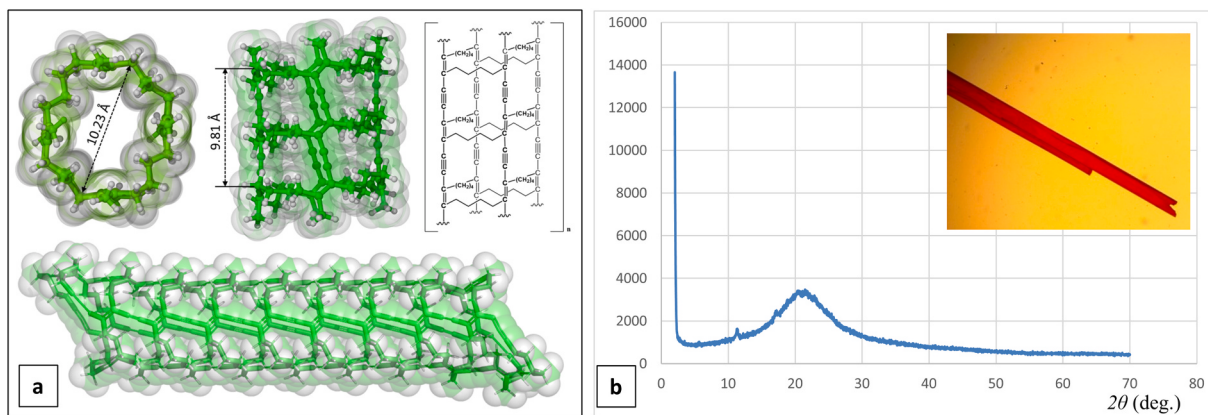


Fig. 4. Panel a: a hypothetical polydiacetylene architecture comprised of 3 individual **DA-4** molecules, view atop and the side view (DFT geometry optimization, B3LYP, 3-21G basis set) and respective 9-cyclic stack (semi-empirical PM3 calculations) featuring alternating C=C double and C≡C triple bonds; panel b: pXRD plot of **DA-4** (inset mage represents UV-254 nm irradiated **DA-4** red crystal).

techniques would be limited to single crystal X-ray analysis, Raman and IR-spectroscopies due to the very low solubility of polydiacetylene (PDA) material in common organic solvents [28]. Gratifyingly, pXRD measurements of UV-irradiated samples as well as their respective FT-IR spectra (broad C=C band at $\sim 1700 \text{ cm}^{-1}$) provided substantial evidence for polymerization of **DA-4** monomer. Panel b of Fig. 4 exhibited one broadened first order reflection peak ($2\theta \sim 20 \text{ deg.}$ with d -spacing $\sim 4.4 \text{ \AA}$) which likely corresponds to the repeat distance between individual hydrocarbon cycles in PDA structure.

Calculations performed on **polyDA-4** scaffold suggested the presence of cavity inside PDA framework as depicted above. We hypothesize that

void space may be filled with solvent guest molecules remaining after “crystal-to-crystal” polymerization. Such ladder-type polymer nanotubes with long conjugation chains may be useful to construct materials for sensing and electronics [25a].

Again, reactive **DA-4** phases obtained by crystallization of diacetylene monomers from 1,4-dioxane and toluene seemed to be prone to 1,4-addition polymerization upon thermal annealing at elevated temperatures, e.g., 100, 140, and 210 °C, as evident by appearance of characteristic band at $\sim 1700 \text{ cm}^{-1}$ in their respective FT-IR spectra (Figures S32–S36).

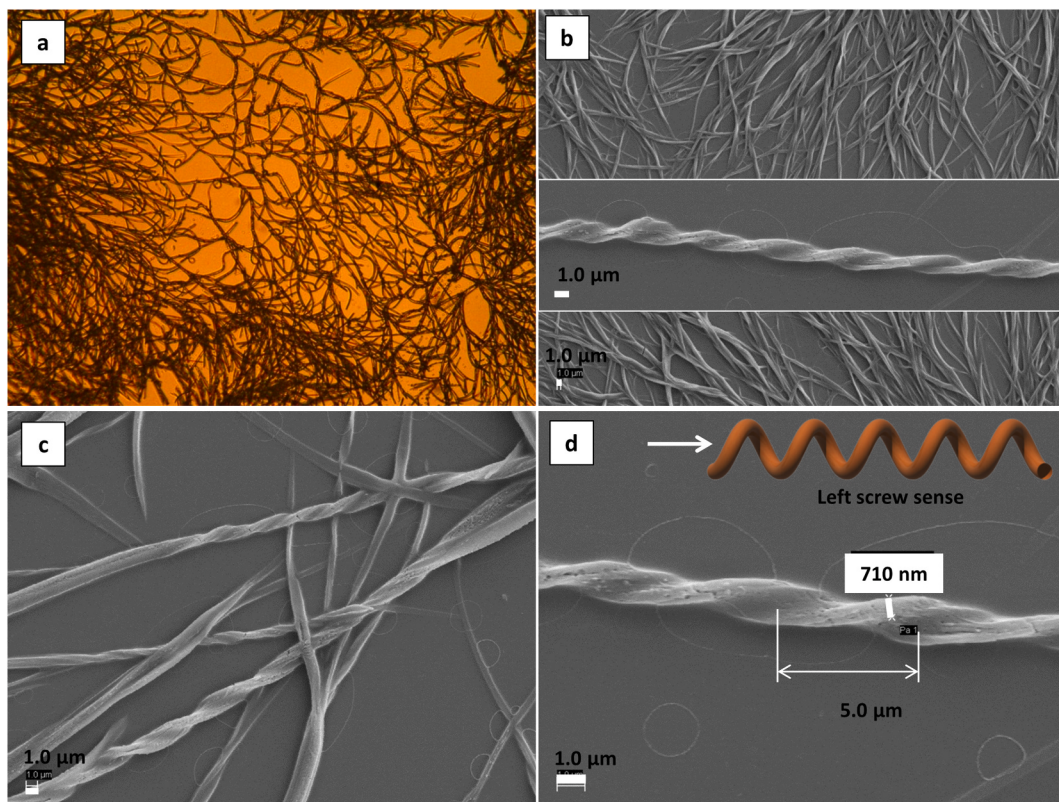


Fig. 5. POM micrograph of partially polymerized **DA-4** monomer deposited from 1,4-dioxane (panel a) and SEM images of **DA-4** deposited from 1,2-dichloroethane (panels b–d, scale bar: 1.0 μm). Slides with deposited material were irradiated with UV-light (20 W, 365 nm, 2 h exposure) and washed with CHCl_3 to remove unreacted monomer.

2.3. PDA secondary structures investigated by POM, AFM, SEM, and TEM analytical techniques

Polarized optical microscopy (POM) images revealed densely packed fibrous branched patterns when **DA-4** stock solutions were deposited on glass slides and allowed to evaporate slowly at ambient temperature (Fig. 5, panel a). We explored possibility of growing these specific intertwined crystals from different solvents including THF, 1,4-dioxane, and toluene (Figures S37–S39) and these morphologies were found to be predominant in a wide range of concentrations. Moreover, we examined aggregation behaviours of **DA-4** diacetylene using SEM imaging (Fig. 5, panels b–d). Thus, we found out that polymerized **DA-4** material from 1,2-dichloroethane may form distinctive secondary structures of both left and right handedness as shown below. More images of this nature are presented in ESI (Figures S40–S43).

It is uncertain at this point what caused the left- and right-handed helix screw sense in polymerized **DA-4** diacetylene. We believe these interesting helical aggregates are both solvent and concentration dependent as changing the solvent from 1,2-dichloroethane to $\text{CHCl}_3/\text{EtOH}$ (10 wt%) binary mixture resulted in short bent fibers (Figure S44) which are somewhat reminiscent of PDA microcrystals obtained by spin-coating of diacetylene macrocycle on the Si wafer followed by thermal treatment as outlined previously [27a]. Other examples of PDA nanotubes and nanowires having bundled structure could be found in the literature [25c,25d]. Noteworthy, authors [27e] were able to acquire high resolution STM images of discrete PDA nanotubes from amphiphilic macrocyclic diacetylene with 3.52 nm width on the HOPG surface.

In fact, helical (or ribbon-like) **DA-4** aggregates persist in a wide range of concentrations, i.e., from 1.25 mg/mL to 10 mg/mL. We hypothesize that higher concentrations caused more extensive aggregation and molecular ordering of **DA-4** monomer units into helical assemblies. The helical pitch, or the distance between identical places on neighboring helical turns, can fluctuate, but estimated to be around $\sim 5 \mu\text{m}$ with a thickness of helical turn of $\sim 710 \text{ nm}$ (Fig. 5d). It is not uncommon for acetylenic species to form chiral secondary structures. Thus, poly(phenylacetylene)s [29,30] are known to be helical as well as there are some precedents in the literature regarding chirality induction in polydiacetylenes [31]. Moreover, diacetylenes afforded helical nanoribbon polydiacetylenes via supramolecular gelation [32] and amphiphilic diacetylenes were found to self-assemble into vesicles and supramolecular gel with helical structure [33]. There is a reason to believe that **DA-4** discrete molecules may similarly generate chiral ribbon-like structures of both handedness when deposited from 1,2-dichloroethane on a substrate surface which further underwent polymerization upon exposure to UV-light. Another plausible explanation of observed unusual aggregation behavior and molecular ordering involves “twisting upon crystallization” phenomenon when chirality imparted to achiral polymers by crystallization process [34]. The results of investigation carried out are suggestive that aggregation behavior of diacetylenic species can be tuned by changing the solvent and concentration of stock solution.

3. Conclusion

Thus, we experimentally confirmed by single crystal X-ray analysis that **DA-4** tetrameric diacetylene obtained during a course of copper-mediated ring closing reaction is prone to self-organize into polymerizable channel-like architectures. Accordingly, we have obtained tubular covalent polydiacetylenes (PDAs), a family of conjugated polymers. Another important experimental finding was that **DA-4** based nanotubes obtained from $\text{CHCl}_3/\text{EtOH}$ solvent mixture do not incorporate template solvent molecules unlike similar tubular assemblies obtained from toluene, mesitylene, and 1,4-dioxane. Finally, discovered polymerized **DA-4** twisted ribbons as well as other secondary structures may result from specific arrangement of the individual **DA-4** molecules followed by formation of ene-yne alternated PDA backbone upon

exposure to UV-light or high temperature. We assume that achiral **DA-4** monomer may assemble into chiral secondary structures identifiable by SEM. Overall, control over fibrillar/ribbon aggregates thickness through varying **DA-4** monomer concentration and solvent change may represent significant interest for potential technological applications as it provides unique, synthetic context to explore successful manipulation of PDA assemblies at molecular level, thus, leading to the synthesis of “carbon-rich” acetylenic materials.

4. Materials and methods

All starting materials were obtained from Sigma-Aldrich, Fluka or TCI America. Thin layer chromatography (TLC) was performed on Sigma-Aldrich TLC Plates (silica gel on aluminum, 200 mm layer thickness, 2–25 mm particle size, 60 Å pore size). Column chromatography was performed using silica gel (230–400 mesh) from Merck. ^1H nuclear magnetic resonance spectra were recorded at 500 MHz on Bruker Avance IIITM 500 instrument at room temperature; ^1H chemical shifts are reported in parts per million (ppm) relative to the corresponding residual solvent peak. Mass-spectra were recorded using Accurate Mass QT of LC/MS instrument at University of Texas at Austin, Chemistry Department Mass Spectrometry Facility.

4.1. X-ray single crystal structure determination of target molecules **DA-3**, **DA-4** and **DA-5**

All data were collected using graphite-monochromated Mo $K\alpha$ radiation ($\lambda = 0.71073 \text{ \AA}$). The structures were solved by direct methods and refined with SHELXL [35], Bruker APEX2 [36] and Olex2 [37,38] software packages: SHELXL2014/7 for **DA-3**, SHELXL2016/6 for **DA-4** from 1,4-dioxane, SHELXL2014/7 for **DA-4** from $\text{CHCl}_3/\text{EtOH}$, SHELXL2014/7 for **DA-4** from mesitylene, SHELXL2016/6 for **DA-4** from toluene, SHELXL2014/7 for **DA-5** from CHCl_3 . Crystallographic data have been deposited with the Cambridge Crystallographic Data Centre, CCDC 1852137 (**DA-3**), 1852138 (**DA-5**), 1852357 (**DA-4** from $\text{CHCl}_3/\text{EtOH}$), 1852358 (**DA-4** from mesitylene), 1852360 (**DA-4** from toluene), 1852361 (**DA-4** from 1,4-dioxane). Copies of the data can be obtained, free of charge, on application to CCDC, 12 Union Road, Cambridge CB2 1EZ, UK (fax: +44-(0)1223–336033 or e-mail: deposit@ccdc.cam.ac.uk).

Single crystal X-ray of **DA-3** from hexane/toluene. Structure: $\text{C}_{24}\text{H}_{24}$. Unit Cell Parameters: $a = 22.2098(8)$, $b = 8.4481(3)$, $c = 10.1908(4)$, $\alpha = 90.00^\circ$, $\beta = 98.697(2)^\circ$, $\gamma = 90.00^\circ$, $V = 1890.12(12) \text{ \AA}^3$, $M_r = 312.43$, $Z = 4$, monoclinic, space group C 1 c 1. Mo $K\alpha$ radiation ($\lambda = 0.71073 \text{ \AA}$), $\mu = 0.062 \text{ mm}^{-1}$, $T = 100(2)\text{K}$. R (reflections) = 0.0348 (3885), wR^2 (reflections) = 0.0776(4339). The goodness of fit on F^2 was 1.031.

Single crystal X-ray of **DA-4** from 1,4-dioxane (structure solution without a solvent). Structure: $\text{C}_{16}\text{H}_{16} \cdot 0.5(\text{C}_{32}\text{H}_{32})$. Unit Cell Parameters: $a = 24.023(3)$, $b = 4.9890(6)$, $c = 27.219(3)$, $\alpha = 90.00^\circ$, $\beta = 112.475(3)^\circ$, $\gamma = 90.00^\circ$, $V = 3014.5(7) \text{ \AA}^3$, $M_r = 208.29$, $Z = 4$, monoclinic, space group C 1 2 1. Mo $K\alpha$ radiation ($\lambda = 0.71073 \text{ \AA}$), $\mu = 0.051 \text{ mm}^{-1}$, $T = 100(2)\text{K}$. R (reflections) = 0.0791(5678), wR^2 (reflections) = 0.1993(6652). The goodness of fit on F^2 was 1.066.

Single crystal X-ray of **DA-4** from $\text{CHCl}_3/\text{EtOH}$. Structure: $\text{C}_{32}\text{H}_{32}$. Unit Cell Parameters: $a = 5.1123(3)$, $b = 8.1034(5)$, $c = 15.6029(9)$, $\alpha = 101.341(2)^\circ$, $\beta = 97.191(2)^\circ$, $\gamma = 103.738(2)^\circ$, $V = 605.52(6) \text{ \AA}^3$, $M_r = 416.57$, $Z = 1$, triclinic, space group P –1. Mo $K\alpha$ radiation ($\lambda = 0.71073 \text{ \AA}$), $\mu = 0.064 \text{ mm}^{-1}$, $T = 100(2)\text{K}$. R (reflections) = 0.0633 (2305), wR^2 (reflections) = 0.1248(2708). The goodness of fit on F^2 was 1.173.

Single crystal X-ray of **DA-4** from mesitylene (structure solution without a solvent). Structure: $\text{C}_{32}\text{H}_{32}$. Unit Cell Parameters: $a = 4.9352(4)$, $b = 26.4828(19)$, $c = 11.2314(9)$, $\alpha = 90^\circ$, $\beta = 91.449(3)^\circ$, $\gamma = 90^\circ$, $V = 1467.5(2) \text{ \AA}^3$, $M_r = 416.58$, $Z = 2$, monoclinic, space group P 1 21/n 1. Mo $K\alpha$ radiation ($\lambda = 0.71073 \text{ \AA}$), $\mu = 0.053 \text{ mm}^{-1}$, $T = 293(2)\text{K}$. R (reflections) = 0.1262 (2019), wR^2 (reflections) = 0.2376(3191). The goodness of fit on F^2 was 1.069.

Single crystal X-ray of **DA-4** from toluene (structure solution without a solvent). Structure: C₃₂H₃₂. Unit Cell Parameters: $a = 5.0299(5)$, $b = 25.890(2)$, $c = 11.0946(11)$, $\alpha = 90^\circ$, $\beta = 92.574(3)^\circ$, $\gamma = 90^\circ$, $V = 1443.3(2)$ Å³, $M_r = 416.58$, $Z = 2$, monoclinic, space group P 1 21/n 1. Mo K α radiation ($\lambda = 0.71073$ Å), $\mu = 0.054$ mm⁻¹, $T = 100(2)$ K. R (reflections) = 0.0569(2517), wR^2 (reflections) = 0.1400(3158). The goodness of fit on F^2 was 1.028.

Single crystal X-ray of **DA-5** from CHCl₃. Structure: C₄₀H₄₀. Unit Cell Parameters: $a = 37.190(3)$, $b = 8.3471(6)$, $c = 10.0031(7)$, $\alpha = 90^\circ$, $\beta = 95.842(2)^\circ$, $\gamma = 90^\circ$, $V = 3089.1(4)$ Å³, $M_r = 520.72$, $Z = 4$, monoclinic, space group C 1 c 1. Mo K α radiation ($\lambda = 0.71073$ Å), $\mu = 0.063$ mm⁻¹, $T = 100.03$ K. R (reflections) = 0.0675(5929), wR^2 (reflections) = 0.1603 (6969). The goodness of fit on F^2 was 1.067.

4.2. Synthesis and characterization of DA-3, DA-4, and DA-5 diacetylenes

Diacetylenes were prepared according to reported procedure using oxidative coupling of 1,7-octadiyne with CuSO₄ in pyridine [26a,c].

To a 2 L three-neck round-bottomed flask equipped with a mechanical stirrer, thermometer, additional funnel, and reflux condenser, 225 g (1.14 mol) of cupric acetate monohydrate, 15.0 g (0.141 mol) of 1,7-octadiyne, and 1.5 L of pyridine were added. Reaction mixture allowed to stir at 43 °C for 4 h, cooled, and filtered. The solids retained on the filter were washed with 100 mL of benzene (three times). The benzene washings were combined with the pyridine filtrate, and solvent was removed under reduced pressure to near dryness. The resulting dark brown residue was extracted with 1.5 L of 40% (v/v) water-benzene mixture. The benzene layer was separated from the aqueous layer and washed with 100 mL of water, 200 mL of 3 N HCl solution (2 times), 200 mL of water, and dried over MgSO₄. Concentration of the solution and drying under reduced pressure provided a dark brown solid which was subjected to a column of SiO₂ using hexanes/benzene (4:1) mixture as an eluent. The desired cyclotetraadiyne monomer (**DA-4**) was isolated by column chromatography along with **DA-2**, **DA-3**, **DA-5**, and **DA-6** cyclic diynes.

Dimeric **DA-2** (cyclohexadeca-1,3,9,11-tetrayne). ¹H NMR (CDCl₃): δ 2.21 (s, 8H), 1.73 (s, 8H); FT-IR (neat): 2948, 2931, 2900, 2859, 2253, 2186, 2140, 1714, 1441, 1454, 1422, 1362, 1318, 1273, 1236, 1176, 1035, 894, 795, 738, 576, 459 cm⁻¹. MS (CI) *m/z*: 208 [M]⁺.

Trimeric **DA-3** (cyclotetracosa-1,3,9,11,17,19-hexayne). ¹H NMR (CDCl₃): δ 2.27 (s, 12H), 1.67 (s, 12H); FT-IR (neat): 2929, 2897, 2862, 2828, 2255, 2164, 1454, 1422, 1366, 1322, 1273, 1029, 735, 434 cm⁻¹. MS (CI) *m/z*: 312 [M]⁺.

Tetrameric **DA-4** (cyclodotriaconta-1,3,9,11,17,19,25,27-octayne). ¹H NMR (CDCl₃): δ 2.26 (s, 16H), 1.68 (s, 16H); FT-IR (neat): 2947, 2921, 2898, 2860, 2826, 2255, 2165, 1756, 1454, 1422, 1366, 1321, 1255, 1170, 1032, 772, 726, 692, 626, 463, 448 cm⁻¹; MS (high res. ESI) *m/z*: 524.16 [M + Ag]⁺.

Pentameric **DA-5** (cyclotetraconta-1,3,9,11,17,19,25,27,33,35-decayne). ¹H NMR (CDCl₃): δ 2.29 (s, 20H), 1.66 (s, 20H); FT-IR (CHCl₃): 2939, 2866, 2260, 2163 cm⁻¹; MS (CI) *m/z*: 521 [M + 1]⁺.

Hexameric **DA-6** (cyclooctatetraconta-1,3,9,11,17,19,25,27,33,35,41,43-dodecayne). ¹H NMR (CDCl₃): δ 2.29 (s, 24H), 1.64 (s, 24H); FT-IR (CHCl₃): 2939, 2866, 2260, 2163 cm⁻¹. MS (CI) *m/z*: 626 [M + 2]²⁺.

4.3. Attempted polymerization of DA-4 monomer using UV-254 handheld lamp and 365 nm (20 Watt) light source

Isolated single crystals (or material deposited on the glass slides and silicon wafers) were irradiated by UV-lamps (254 nm or 365 nm) for ~12 h. Generally, the crystals were found unacceptable to run single crystal X-ray determination after long UV-light exposure. Solid material on glass slides (or silicon wafers) was gently rinsed with chloroform several times to remove unreacted monomer and soluble oligomers before preparing specimens for SEM analysis.

Credit author statement

Oleg V. Kulikov: Conceptualization, Methodology, Software, Formal analysis, Writing – original draft. Arshad Mehmood: Visualization, single crystal X-ray analysis (data collection) and structural refinement. Yulia V. Sevryugina: single crystal X-ray analysis and structural refinement.

Declaration of competing interest

The authors declare that they have no known competing financial interests or personal relationships that could have appeared to influence the work reported in this paper.

Acknowledgements

Funding for this work was provided by the Faculty start-up fund from the University of Texas at Dallas (UTD) and the Endowed Chair for Excellence at UTD. We gratefully acknowledge the NSF-MRI grant (CHE-1126177) used to purchase the Bruker Advance III 500 NMR instrument.

Appendix A. Supplementary data

Supplementary data to this article can be found online at <https://doi.org/10.1016/j.rinma.2022.100262>.

References

- [1] J.-H. Ryu, N.-K. Oh, M. Lee, Tubular assembly of amphiphilic rigid macrocycle with flexible dendrons, *Chem. Commun.* (2005) 1770–1772.
- [2] Y. Zhong, Y. Yang, Y. Shen, W. Xu, Q. Wang, A.L. Connor, X. Zhou, L. He, X. C. Zeng, Z. Shao, Z.-L. Lu, B. Gong, Enforced tubular assembly of electronically different hexakis(m-phenylene ethynylene) macrocycles: persistent columnar stacking driven by multiple hydrogen-bonding interactions, *J. Am. Chem. Soc.* 139 (44) (2017) 15950–15957.
- [3] M. Petryk, A. Janiak, M. Kwit, Unexpected formation of a tubular architecture by optically active pure organic calixsalen, *CrystEngComm* 19 (2017) 5825–5829.
- [4] Y. Zhen, K. Inoue, Y. Wang, T. Kusamoto, K. Nakabayashi, S.-I. Ohkoshi, W. Hu, Y. Guo, K. Harano, E. Nakamura, Acid-responsive conductive nanofiber of tetrabenzoporphyrin made by solution processing, *J. Am. Chem. Soc.* 140 (1) (2018) 62–65.
- [5] Q. Wang, Y. Zhong, D.P. Miller, X. Lu, Q. Tang, Z.-L. Lu, E. Zurek, R. Liu, B. Gong, Self-Assembly and molecular recognition in water: tubular stacking and guest-templated discrete assembly of water-soluble, shape-persistent macrocycles, *J. Am. Chem. Soc.* 142 (6) (2020) 2915–2924.
- [6] S.T. Schneebeli, C. Cheng, K.J. Hartlieb, N.L. Strutt, A.A. Sarjeant, C.L. Stern, J. F. Stoddart, Asararenes—a family of large aromatic macrocycles, *Chem. Eur. J.* 19 (2013) 3860–3868.
- [7] S. Negin, M.M. Daschbach, O.V. Kulikov, N. Rath, G.W. Gokel, Pore formation in phospholipid bilayers by branched-chain pyrogallol[4]arenes, *J. Am. Chem. Soc.* 133 (10) (2011) 3234–3237.
- [8] H. Kumari, S.R. Kline, W.G. Wycoff, J.L. Atwood, Investigating structural alterations in pyrogallol[4]arene-pyrene nanotubular frameworks, *Small* 8 (21) (2012) 3321–3325.
- [9] S. Matsubara, H. Tamiaki, Phototriggered dynamic and biomimetic growth of chlorosomal self-aggregates, *J. Am. Chem. Soc.* 141 (3) (2019) 1207–1211.
- [10] A.V. Mossine, H. Kumari, D.A. Fowler, A. Shih, S.R. Kline, C.L. Barnes, J.L. Atwood, Ferrocene species included within a pyrogallol[4]arene Tube, *Chem. Eur. J.* 18 (33) (2012) 10258–10260.
- [11] M. Suzuki, J.F.K. Kotyk, S.I. Khan, Y. Rubin, Directing the crystallization of dehydro[24]annulenes into supramolecular nanotubular scaffolds, *J. Am. Chem. Soc.* 138 (18) (2016) 5939–5956.
- [12] B.A. DeHaven, H.K. Liberatore, A. Greer, S.D. Richardson, L.S. Shimizu, Probing the formation of reactive oxygen species by a porous self-assembled benzophenone bis-urea host, *ACS Omega* 4 (5) (2019) 8290–8298.
- [13] M.N. Tahir, A. Nyayachavadi, J.-F. Morin, S. Rondeau-Gagne, Recent progress in the stabilization of supramolecular assemblies with functional polydiacetylenes, *Polym. Chem.* 9 (2018) 3019–3028.
- [14] A. Lapini, S. Fanetti, M. Sittoni, R. Bini, C.-O. Gilbert, S. Rondeau-Gagne, J.-F. Morin, Topochemical polymerization of phenylacetylene macrocycles under pressure, *J. Phys. Chem. C* 122 (34) (2018) 20034–20039.
- [15] R.R. Chance, J.M. Sowa, An examination of the thermal polymerization of a crystalline diacetylene using diffuse reflectance spectroscopy, *J. Am. Chem. Soc.* 99 (20) (1977) 6703–6708.
- [16] J. Tang, M. Weston, R.P. Kuchel, F. Lisi, K. Liang, R. Chandrawati, Fabrication of polydiacetylene particles using a solvent injection method, *Mater. Adv.* 1 (6) (2020) 1745–1752.

- [17] T.C. Pham, S. Lee, D. Kim, O.-S. Jung, M.W. Lee, S. Lee, Visual simultaneous detection and real-time monitoring of cadmium ions based on conjugated polydiacetylenes, *ACS Omega* 5 (48) (2020) 31254–31261.
- [18] (a) G. Shin, M.I. Khazi, J.-M. Kim, Protonation-triggered supramolecular gel from macrocyclic diacetylene: gelation behavior, topochemical polymerization, and colorimetric response, *Langmuir* 36 (46) (2020) 13971–13980;
 (b) B.P. Krishnan, S. Raghu, S. Mukherjee, K.M. Sureshan, Organogel-assisted topochemical synthesis of multivalent glyco-polymer for high-affinity lectin binding, *Chem. Commun.* 52 (98) (2016) 14089–14092.
- [19] M. Weston, R.P. Kuchel, R. Chandrawati, Digital analysis of polydiacetylene quality tags for contactless monitoring of milk, *Anal. Chim. Acta* 1148 (2021), 238190.
- [20] Y.K. Kim, T.C. Pham, J. Kim, C. Bae, Y. Choi, M.H. Jo, S. Lee, Polydiacetylenes containing 2-picolylamide chemosensor for colorimetric detection of cadmium ions, *Bull. Kor. Chem. Soc.* 42 (2) (2021) 265–269.
- [21] (a) J. Liang, L. Huang, N. Li, Y. Huang, Y. Wu, S. Fang, J. Oh, M. Kozlov, Y. Ma, F. Li, R. Baughman, Y. Chen, Electromechanical actuator with controllable motion, fast response rate, and high-frequency resonance based on graphene and polydiacetylene, *ACS Nano* 6 (5) (2012) 4508–4519;
 (b) S. Tian, H. Li, Z. Li, H. Tang, M. Yin, Y. Chen, S. Wang, Y. Gao, X. Yang, F. Meng, J.W. Lauher, P. Wang, L. Luo, Polydiacetylene-based ultrastrong bioorthogonal Raman probes for targeted live-cell Raman imaging, *Nat. Commun.* 11 (2020) 81;
 (c) Q. Huang, W. Wu, K. Ai, J. Liu, Highly sensitive polydiacetylene ensembles for biosensing and bioimaging, *Front. Chem.* 8 (2020), 565782.
- [22] M.N. Tahir, E. Abdulhameid, A. Nyayachavadi, M. Selivanova, S.H. Eichhorn, S. Rondeau-Gagne, Topochemical polymerization of a nematic tetraazaporphyrin derivative to generate soluble polydiacetylene nanowires, *Langmuir* 35 (47) (2019) 15158–15167.
- [23] M.J. Kim, S. Angupillai, K. Min, M. Ramalingam, Y.-A. Son, Tuning of the topochemical polymerization of diacetylenes based on an odd/even effect of the peripheral alkyl chain: thermochromic reversibility in a thin film and a single-component ink for a fountain pen, *ACS Appl. Mater. Interfaces* 10 (29) (2018) 24767–24775.
- [24] (a) R.S. Jordan, Y. Wang, R.D. McCurdy, M.T. Yeung, K.L. Marsh, S.I. Khan, R. B. Kaner, Y. Rubin, Synthesis of graphene nanoribbons via the topochemical polymerization and subsequent aromatization of a diacetylene precursor, *Inside Chem.* 1 (2016) 78–90;
 (b) R.H. Baughman, K.C. Yee, Cyclically-bound ladder polymers of cyclic diacetylene tetramers, US Patent 3 (1975), 923,622 A;
 (c) R.H. Baughman, M.C. Biewer, J.P. Ferraris, J.S. Lamba, Topochemical strategies and experimental results for the rational synthesis of carbon nanotubes of one specified type, *Synth. Met.* 141 (2004) 87–92.
- [25] (a) Y. Xu, M.D. Smith, M.F. Geer, P.J. Pellechia, J.C. Brown, A.C. Wibowo, L. S. Shimizu, Thermal reaction of a columnar assembled diacetylene macrocycle, *J. Am. Chem. Soc.* 132 (15) (2010) 5334–5335;
 (b) G. Shin, M.I. Khazi, J.-M. Kim, Protonation-induced self-assembly of flexible macrocyclic diacetylene for constructing stimuli-responsive polydiacetylene, *Macromolecules* 53 (1) (2020) 149–157;
 (c) J.-M. Heo, Y. Kim, S. Han, J.F. Joung, S. Lee, S. Han, J. Noh, J. Kim, S. Park, H. Lee, Y.M. Choi, Y.-S. Jung, J.-M. Kim, Chromogenic tubular polydiacetylenes from topochemical polymerization of self-assembled macrocyclic diacetylenes, *Macromolecules* 50 (3) (2017) 900–913;
 (d) G. Shin, M.I. Khazi, U. Kundapur, B. Kim, Y. Kim, C.W. Lee, J.-M. Kim, Cation-directed self-assembly of macrocyclic diacetylene for developing chromogenic polydiacetylene, *ACS Macro Lett.* 8 (5) (2019) 610–615.
- [26] (a) F. Sondheimer, Y. Amiel, R. Wolovsky, Unsaturated macrocyclic compounds. VIII.1 Oxidation of terminal diacetylenes to large ring polyacetylenes with cupric acetate in pyridine. Synthesis of five new macrocyclic rings, *J. Am. Chem. Soc.* 81 (17) (1959) 4600–4606;
- (b) A. Banerjie, J.B. Lando, K.C. Yee, R.H. Baughman, Characterization of the ladder polymerization of a crystalline cyclotetradiyne monomer, *J. Polymer Sci., Polymer Phys.* 17 (1979) 655–662;
 (c) K.C. Yee, Solid-state synthesis of a ladder polymer, *J. Polymer Sci. Polymer Chem.* 17 (1979) 3637–3646.
- [27] (a) W.L. Xu, M.D. Smith, J.A. Krause, A.B. Greytak, S. Ma, C.M. Read, L. S. Shimizu, Single crystal to single crystal polymerization of a self-assembled diacetylene macrocycle affords columnar polydiacetylenes, *Cryst. Growth Des.* 14 (2014) 993–1002;
 (b) C. Kantha, H. Kim, Y. Kim, J.-M. Heo, J.F. Joung, S. Park, J.-M. Kim, Topochemical polymerization of macrocyclic diacetylene with a naphthalene moiety for a tubular-shaped polydiacetylene chromophore, *Dyes Pigments* 154 (2018) 199–204;
 (c) K. Bae, J.M. Heo, M.I. Khazi, J.F. Joung, S. Park, Y. Kim, J.-M. Kim, Macrocyclic diacetylene–terthiophene cocrystal: molecular self-assembly, topochemical polymerization, and energy transfer, *Cryst. Growth Des.* 20 (1) (2020) 434–441;
 (d) J. Nagasawa, M. Yoshida, N. Tamaoki, Synthesis, gelation properties and photopolymerization of macrocyclic diacetylenedicarboxamides derived from L-glutamic acid and trans-1,4-cyclohexanediol, *Eur. J. Org. Chem.* 12 (2011) 2247–2255;
 (e) J.-M. Heo, Y. Son, S. Han, H.-J. Ro, S. Jun, U. Kundapur, J. Noh, J.-M. Kim, Thermochromic polydiacetylene nanoparticle from amphiphilic macrocyclic diacetylene in aqueous solution, *Macromolecules* 52 (11) (2019) 4405–4411.
- [28] As a matter of fact, diffusion NMR (DECRA analysis, DMSO-d₆) as well as GPC (DMF) data did not provide sufficient evidence for polymerization induced by UV-light (UV-254 nm lamp or LED UV, 3 days) as well as by thermal annealing (120 °C, 12 hr) due to mostly insoluble nature of polymer. GPC showed no integrable peaks in polymerized DA-4 samples or exhibited very low intensity peaks with number average molecular weight (M_n) ~ 1.9 kDa.
- [29] K. Maeda, S. Wakasone, K. Shimomura, T. Ikai, S. Kanoh, Chiral amplification in polymer brushes consisting of dynamic helical polymer chains through the long-range communication of stereochemical information, *Macromolecules* 47 (19) (2014) 6540–6546.
- [30] S. Ohsawa, S. Sakurai, K. Nagai, M. Banno, K. Maeda, J. Kumaki, E. Yashima, Hierarchical amplification of macromolecular helicity of dynamic helical poly(phenylacetylene)s composed of chiral and achiral phenylacetylenes in dilute solution, liquid crystal, and two-dimensional crystal, *J. Am. Chem. Soc.* 133 (1) (2011) 108–114.
- [31] G. Yang, S. Zhang, J. Hu, M. Fujiki, G. Zou, The chirality induction and modulation of polymers by circularly polarized light, *Symmetry* 11 (4) (2019) 474.
- [32] C. Chen, J. Chen, T. Wang, M. Liu, Fabrication of helical nanoribbon polydiacetylene via supramolecular gelation: circularly polarized luminescence and novel diagnostic chiroptical signals for sensing, *ACS Appl. Mater. Interfaces* 8 (44) (2016) 30608–30615.
- [33] S. Li, L. Zhang, J. Jiang, Y. Meng, M. Liu, Self-assembled polydiacetylene vesicle and helix with chiral interface for visualized enantioselective recognition of sulfonamide, *ACS Appl. Mater. Interfaces* 9 (42) (2017) 37386–37394.
- [34] M. Rosenthal, G. Bar, M. Burghammer, D.A. Ivanov, On the nature of chirality imparted to achiral polymers by the crystallization process, *Angew. Chem. Int. Ed.* 50 (38) (2011) 8881–8885.
- [35] G.M. Sheldrick, A short history of SHELX, *Acta Crystallogr. A* 64 (2008) 112–122.
- [36] Bruker, APEX2 Software Package, V. 1.27. Bruker Molecular Analysis Research Tool, Bruker AXS, Madison, Wisconsin, USA, 2005.
- [37] O.V. Dolomanov, L.J. Bourhis, R.J. Gildea, J.A.K. Howard, H. Puschmann, OLEX2: a complete structure solution, refinement and analysis program, *J. Appl. Crystallogr.* 42 (2009) 339–341.
- [38] Compiled, 05.29 svn.r3508 for OlexSys, GUI svn.r5506, 2018.